applied sciences

MDPI

Article

Numerical Simulation Research and Design Optimization of a Single-Column Shield Hydraulic Support Model Based on a Double-Column Shield Hydraulic Support

Dong An, Zhiyang Wang, Hailiang Xu *, Jiawei Tu and Runsong Tang

School of Civil Engineering, North China University of Technology, Beijing 100144, China; andong@ncut.edu.cn (D.A.); 19816003505@163.com (Z.W.); tujiawei801@gmail.com (J.T.); tangrs15590981015@163.com (R.T.)
* Correspondence: xuhailiang@ncut.edu.cn

Abstract

This paper presents a systematic comparative study on the mechanical performance of ZY6000 single-column and ZY6400 double-column shield hydraulic supports using SolidWorks 3D modeling and Abaqus explicit dynamic finite element simulation. High-precision numerical models of both supports were established, and three typical working conditions (canopy two-end loading, base two-end loading, and canopy eccentric loading) were designed to evaluate their stress distribution, displacement characteristics, bearing capacity, and structural stability. The transient response laws of the canopy and base under impact loads were quantitatively analyzed, and targeted structural optimizations were proposed for the ZY6000 support. The results show that the ZY6000 single-column support exhibits superior canopy mechanical performance, with an 8.77% reduction in maximum canopy stress compared to the ZY6400 support. After optimization, the maximum base stress of the ZY6000 support was reduced by 25.3%, significantly improving its structural safety margin. This study verifies the engineering feasibility of single-column shield hydraulic supports and provides valuable references for the lightweight design of mining support equipment.

Keywords: structural design; hydraulic support; transient dynamics; simulation

1. Introduction

Hydraulic support [1–9] serves as the core supporting equipment for fully mechanized coal mining faces. Its structural mechanical properties, kinematic attitude stability, and dynamic response of the hydraulic system directly govern the underground support safety, mining efficiency, and service life of the equipment [10–13]. Under the combined effects of complex geological conditions, impact loads [14,15], hydraulic supports are prone to problems such as lateral instability, and stress concentration in the canopy. Traditional theoretical calculations and physical prototype tests have inherent limitations in conducting full-condition, multi-factor, and high-precision analysis of transient dynamic characteristics [16–20]. Theoretical calculations often rely on simplified assumptions and cannot accurately reflect complex stress distributions and dynamic responses, while physical prototype tests are costly, time-consuming, and difficult to replicate extreme working conditions. Nevertheless, these approaches remain irreplaceable for model validation, parameter calibration, and establishing design benchmarks. Numerical simulation, with its advantages of repeatability, low cost, and full-parameter visualization, provides a powerful comple-

Check for updates

Academic Editor: Arkadiusz Gola

Received: 22 May 2026
Revised: 16 June 2026
Accepted: 17 July 2026
Published: 27 July 2026

Copyright: © 2026 by the authors. Licensee MDPI, Basel, Switzerland. This article is an open access article distributed under the terms and conditions of the Creative Commons Attribution (CC BY) license.

mentary tool for the design optimization, performance prediction, and failure mechanism investigation of hydraulic supports.

Recently, domestic and international scholars have conducted multi-dimensional research on the numerical simulation of hydraulic supports. Wang et al. [21] performed transient dynamic simulations on a cyclic self-moving combined support, revealing the stress and deformation laws of the canopy under uniform, concentrated, eccentric, and torsional loads, and pinpointing the stress-concentrated regions and structural reinforcement orientations. However, their study only verified a single structural model and did not provide comparative analysis between different support configurations. Liu et al. [19] established a refined finite element model of the ZY14790/15/25D hydraulic support column, which was manufactured by China Coal Beijing Coal Mining Machinery Co., Ltd. (Beijing, China), considering welding, threaded connections, and contact nonlinearity, and conducted dynamic response simulations under multi-condition impact loads. Nevertheless, their research was limited to double-column supports and did not involve single-column configurations. The results show that the stress of key components of the column undergoes a three-stage variation, with prominent stress concentrations in the secondary guide sleeve and the middle cylinder, providing a basis for the structural optimization of the support. Zeng et al. [22] established a mechanical-hydraulic co-simulation platform for hydraulic supports, constructed a rigid–flexible coupled impact dynamics model, and revealed the influence laws of roof rotation position and safety valve hysteresis effect. The results show that backward movement of the roof rotation position can reduce the support column pressure, while safety valve hysteresis will increase the column pressure and hinge impact coefficient, providing a basis for the impact-resistant design of supports. The working face hydraulic support generally adopts a shield-type hydraulic support, as shown in Figure 1.



(**a**) (**b**)

Figure 1. Hydraulic support at the working face. (**a**) Double-column shield hydraulic support. (**b**) Application of shield hydraulic supports in mines.

Despite significant progress in numerical simulation of hydraulic supports, three critical research gaps remain unaddressed:

1. Most existing studies focus on performance optimization of single-type supports, but lack systematic mechanical performance comparison based on the same structural benchmark. This leads to a lack of direct quantitative basis for engineering selection between single-column and double-column supports.
2. Majority of studies only analyze static characteristics under uniform loads, while insufficient attention is paid to transient dynamic responses under extreme conditions such as impact loads and eccentric loads, which are common in underground mining.
3. The strength verification and applicable boundaries of single-column shield hydraulic supports have not been fully demonstrated, limiting their engineering promotion.

Currently, China's coal industry is facing the dual challenges of cost reduction and green mining. Traditional double-column shield hydraulic supports have obvious limitations in medium-thickness coal seams with light loads: complex structure, heavy weight, high manufacturing cost, numerous hydraulic pipelines and high maintenance difficulty. The performance redundancy of double-column supports in these working faces can reach 20–30%, significantly increasing mining costs.

In contrast, single-column shield hydraulic supports can reduce manufacturing costs by 15–20% and overall weight by 10–15% by reducing the number of columns and hydraulic components. However, further research and verification are required to confirm whether the bearing capacity and stability of the single-column support can meet the practical engineering requirements.

This paper takes the ZY6000 single-column shield hydraulic support and ZY6400 double-column shield hydraulic support (China Coal Beijing Coal Mining Machinery Co., Ltd., Beijing, China) as the research objects, and conducts modeling and finite element simulation research based on Solidworks (v2025) and Abaqus (v2024) software. The main research objectives are as follows: (1) Establish accurate finite element models of ZY6000 single-column and ZY6400 double-column shield hydraulic supports using Solidworks modeling software, optimize simulation parameters, and improve the accuracy of the simulation models; (2) systematically compare the mechanical properties (stress distribution, displacement characteristics, load-bearing capacity, stability) of the two types of supports under the same working conditions, and clarify their mechanical performance differences and applicable boundaries; and (3) while verifying that the ZY6000 single-column shield hydraulic support meets requirements, such as strength, efforts shall be made to minimize the cost requirements of the hydraulic support.

2. Theoretical Basis and Finite Element Model Establishment

2.1. Establishment of Models Shield Hydraulic Supports

In this paper, the ZY6000 single-column shield hydraulic support is modified and designed based on the dimensions of the ZY6400 double-column shield hydraulic support (Figure 2). During the modeling of the hydraulic support, the support requirements of the working face during coal seam mining are taken into account, while ensuring its feasibility and stability in practical engineering applications. SolidWorks software is employed to establish a detailed model of the support dimensions, including the assembly of individual components, in preparation for subsequent simulation and analysis.

As shown in Figure 3. In terms of hydraulic column parameters: The ZY6400 model equips two identical three-stage telescopic columns; each column has segment diameters of ϕ210 mm, ϕ290 mm, ϕ380 mm, with a single column mass of 1035 kg and total column assembly mass of 2070 kg. The ZY6000 design replaces the two small-diameter columns with one enlarged three-stage telescopic column, whose segment diameters are increased to ϕ310 mm, ϕ390 mm, ϕ480 mm to bear the full rated working resistance. The mass of this single enlarged column is 1960 kg, which is 110 kg lighter than the total double-column mass of ZY6400 (2070 kg). Correspondingly, the rated working resistance is adjusted from 6400 kN (ZY6400) to 6000 kN (ZY6000), and the matching hydraulic pipeline and control valve sets are simplified for the single-column system.

This controlled modification scheme isolates the column configuration as the only core variable, eliminating interference from other geometric or boundary differences when comparing mechanical performance between single-column and double-column support structures.

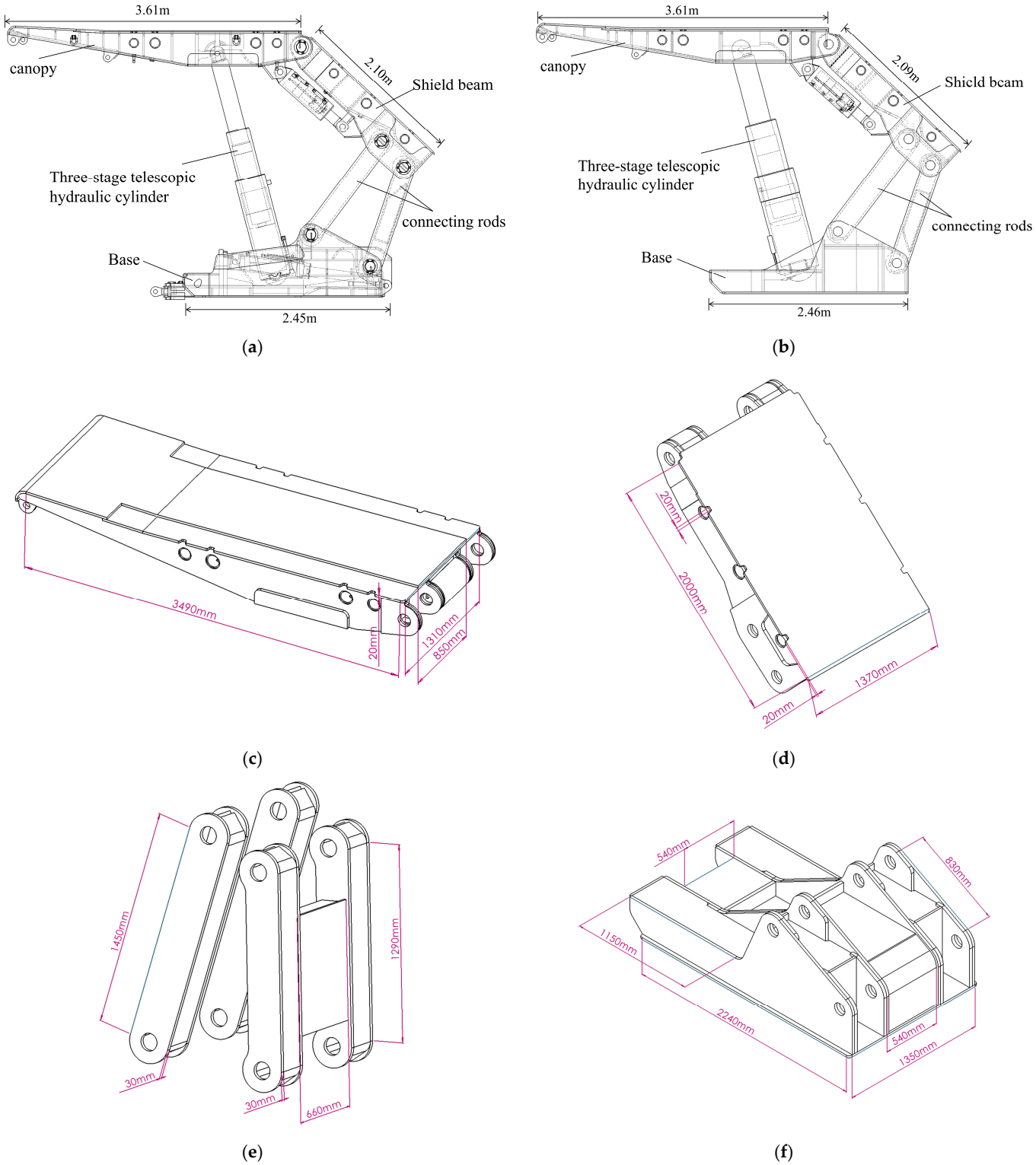

Figure 2. Hydraulic support dimension drawing. (**a**) ZY6400 double-column shield hydraulic support. (**b**) ZY6000 single-column shield hydraulic support. (**c**) Canopy of ZY6000 single-column shield hydraulic support. (**d**) Shield beam of ZY6000 single-column shield hydraulic support. (**e**) Connecting rods of ZY6000 single-column shield hydraulic support. (**f**) Base of ZY6000 single-column shield hydraulic support.

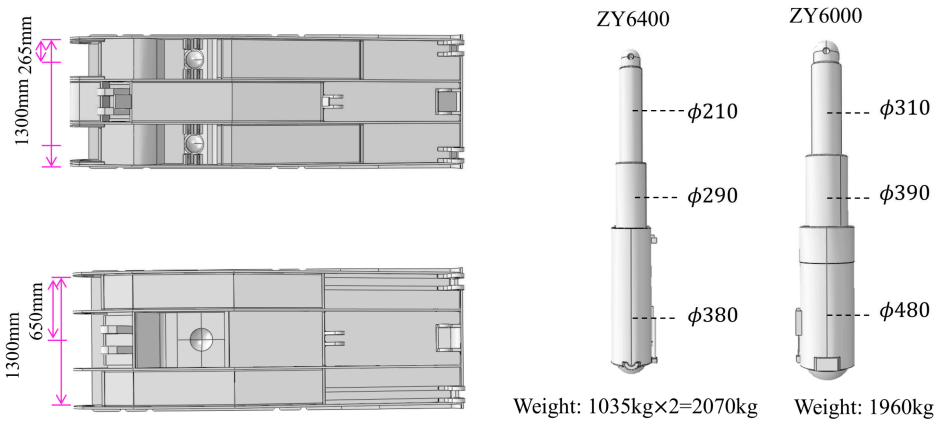

Figure 3. Structural comparison of core modified components between ZY6400 double-column and ZY6000 single-column hydraulic supports, including base column socket layout and dimensional parameters, and dimensional specifications and mass of three-stage telescopic hydraulic columns.

The ZY6400 model is taken as the typical representative of the series, and its core support performance parameters are presented in Table 1, which covers the key indicators determining the support stability and adaptability to mining conditions.

Table 1. Specifications for the ZY6400 double-column shield hydraulic support.

Parameter Item	ZY6400	ZY6000	Description
Working Resistance	6400 kN	6000 kN	Rated support capacity (system pressure P = 39.8 MPa)
Setting Load	5050 kN	4720 kN	Initial support force at rated pump station pressure
Support Height	2350–4500 mm	2350–4500 mm	Minimum and maximum adjustable support height
Support Width	1430–1600 mm	1430–1600 mm	Transverse adaptive range of the support
Center Distance	1500 mm	1500 mm	Center spacing between two adjacent supports
Adaptable Coal Seam Inclination	<15°	<15°	Maximum applicable dip angle of coal seam
Pump Station Pressure	31.4 MPa	31.4 MPa	Rated working pressure of the hydraulic system

2.2. Components of the Hydraulic Support

A shield hydraulic support mainly consists of a canopy, shield, base, hydraulic columns and a linkage mechanism system. The canopy is used to support the roof strata, while the shield plays a key role in isolating the goaf and preventing gangue from falling. The base bears and transfers loads to the floor. The hydraulic columns provide the main supporting force, and the linkage mechanism ensures coordinated movement and stable attitude of the whole support during operation. The two hydraulic supports were modeled in SolidWorks software, and the three-dimensional models were imported into Abaqus for finite element analysis (Figure 4). To improve computational efficiency while ensuring core mechanical accuracy, non-critical load-bearing components (including lifting rings, electrical circuit devices, and auxiliary fasteners with diameters less than 20 mm) were removed from the model. These components do not participate in the main load transfer path of the hydraulic support, which consists of the canopy, shield, base, columns, and linkage mechanism.

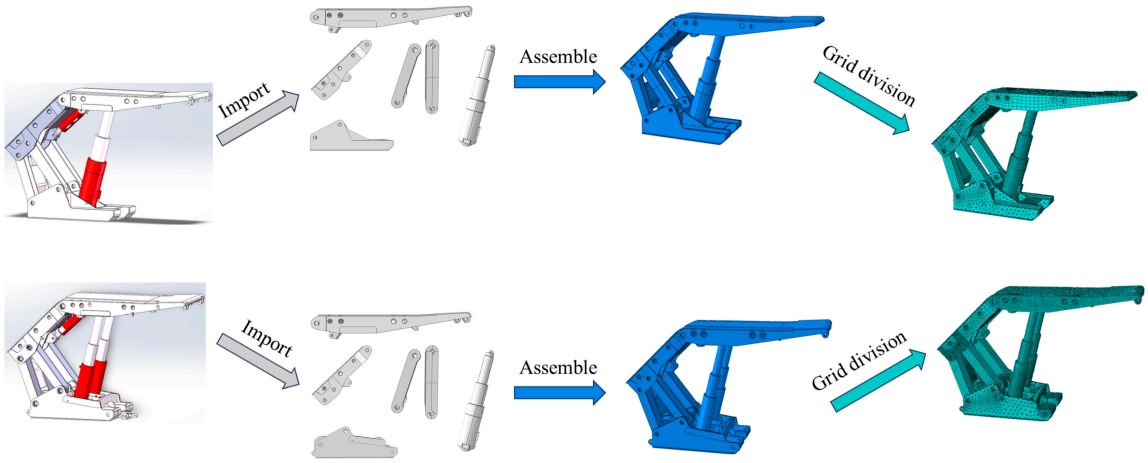

Figure 4. The process of creating a 3D model for finite element simulation of hydraulic supports.

Removing these non-load-bearing components introduces a relative error of less than 2% in the maximum stress and displacement results of core components. A sensitivity analysis was also conducted, which confirmed that retaining these components would change the maximum base stress by only 1.7% and the maximum canopy stress by 1.2%, verifying the negligible influence of these simplifications.

2.3. Material Properties and Mesh Generation of Hydraulic Support Model

In this study, the Q690 high-strength steel used for all core components of the hydraulic support was modeled as an isotropic linear elastic material. The mechanical properties of Q690 steel are shown in Table 2. The linear elastic model was adopted because the maximum equivalent stress in all simulation conditions is less than the yield strength of Q690 steel, and the structure remains in the elastic deformation stage. For conditions where the stress exceeds the yield strength, an elastoplastic model should be used in future studies to accurately predict the plastic deformation and failure behavior of the structure.

Table 2. Mechanical properties of material.

Material Name	Poisson's Ratio	Density/kg/m^3	Elastic Modulus/GPa	Yield Strength/MPa
Q690 steel	0.3	7850	206	690

In this paper, the numerical model of the entire hydraulic support was established and simulated based on the Abaqus/Explicit explicit dynamic solver, and the mesh discretization of the model was carried out in strict accordance with the calculation stability and accuracy requirements of explicit analysis, combined with the geometric structure characteristics, stress distribution and contact action areas of the hydraulic support.

To verify mesh convergence, five mesh sizes (40 mm, 50 mm, 60 mm, 70 mm, and 80 mm) were tested for all three critical load-bearing components (canopy, base, and shield) under all three working conditions. The maximum Mises stress of each component was taken as the convergence indicator, and the relative error was calculated using the 40 mm fine mesh result as the reference value.

$$\text{Relative Error} = \left| \frac{\sigma_{mesh} - \sigma_{40}}{\sigma_{40}} \right| \times 100\% \quad (1)$$

As shown in Figure 5, taking the meshing of different sizes for the base of the hydraulic support as an example, it can be clearly observed that the coarser the mesh, the

monotonically increasing trend of the difference in simulation results. The calculation results show that when using a 60 mm mesh size, the maximum relative error is 4.1% for the base, 3.8% for the canopy, and 3.5% for the shield, with a comprehensive average error of 3.8%. When the mesh size is reduced to 50 mm, the error decreases to less than 2%, but the computational time increases by 65%. Considering the balance between accuracy and efficiency, a 60 mm mesh size was selected for all components.

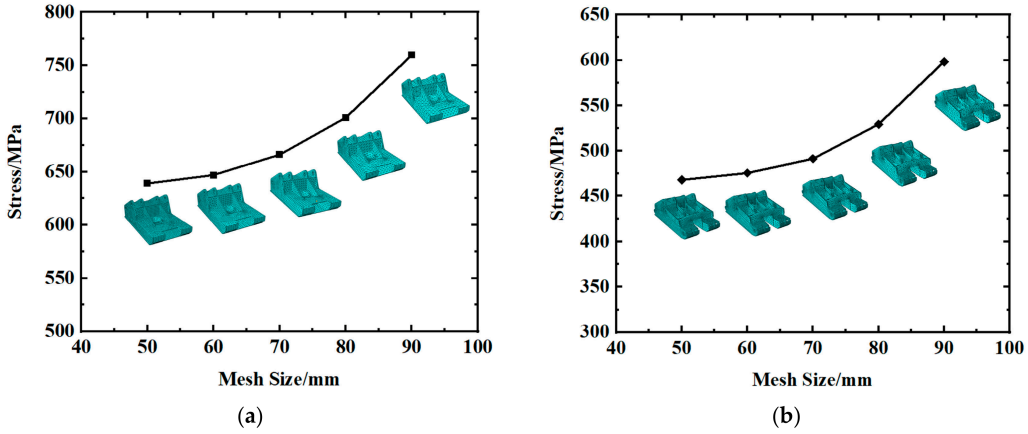

Figure 5. Mesh generation for hydraulic support base. (**a**) Base of ZY6000 single-column shield hydraulic support. (**b**) Base of ZY6400 double-column shield hydraulic support.

After mesh integration and quality inspection, no severely distorted elements, negative volume elements or elements with excessive aspect ratio existed in the overall model, and the mesh quality fully met the calculation requirements of Abaqus/Explicit, effectively guaranteeing the stability of the calculation process and the reliability of the results. Upon completion of model discretization, the total number of finite elements for the ZY6400 double-column shield hydraulic support and ZY6000 single-column shield hydraulic support was 262,862 and 238,753, respectively. The mesh nodes were uniformly arranged, the mesh matching of each structural component was satisfactory, and no mesh discontinuity was observed.

2.4. Setting of Different Working Conditions

All loading conditions in this study are designed in accordance with the coal industry standard, "Powered support for coal mine—Part 1: General specification" (GB 25974.1-2010) [23], which specifies the test methods and loading requirements for the strength verification of hydraulic supports.

(1) Rectangular rigid padding blocks with dimensions of 150 mm × 50 mm × 1500 mm are arranged at both ends of the hydraulic support canopy, at a distance of d = 35 mm from the end boundaries of the canopy. A total load of 1.2 times the working resistance (1.2 × 6000 kN = 7200 kN) is applied to the two padding blocks. Set the base of the hydraulic support to be fully fixed. This working condition is established to analyze and compare the mechanical behaviors of the canopies of two hydraulic supports.

(2) Rectangular rigid padding blocks with dimensions of 150 mm × 50 mm × 1500 mm are placed at both ends of the hydraulic support base, at a distance of d = 35 mm from the end boundaries of the base. A total load of 1.2 times the working resistance (1.2 × 6000 kN = 7200 kN) is exerted on the two padding blocks. Set the column socket of the base as a fully fixed boundary condition. This condition is configured to investigate and compare the stress distributions of the bases of two hydraulic supports.

(3) A rectangular rigid padding block with dimensions of 200 mm × 50 mm × 1500 mm is installed on one side of the hydraulic support canopy, at a distance of 0.1 B = 137 mm

from the lateral edge of the canopy. A load of 1.2 times the working resistance (1.2 × 6000 kN = 7200 kN) is applied to the padding block. Set the base of the hydraulic support to be fully fixed. If the lateral rotation angle of the canopy exceeds 8°, the applied load shall be adjusted to the value corresponding to a rotation angle of 8°. Schematic diagrams of all working conditions are presented in Figure 6.

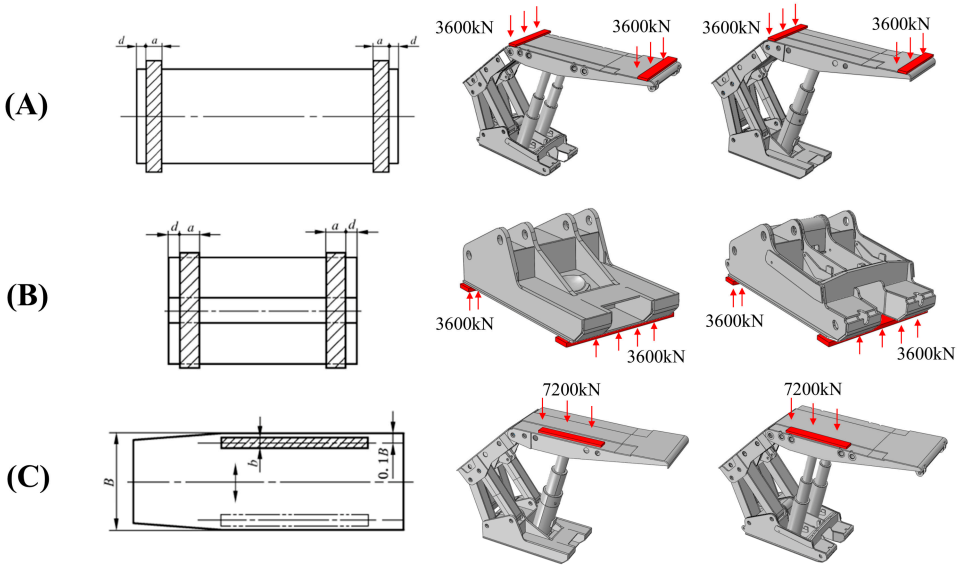

Figure 6. Position of the impact load. (**A**) Loading applied to both ends of the canopy. (**B**) Loading applied to both ends of the base. (**C**) Eccentric loading of canopy. a = 150 mm, b = 200 mm, d = 20~50 mm, and B represents the width of the hydraulic support canopy.

A unified load of 7200 kN (1.2 times the working resistance of the ZY6000 support) was applied to both supports to directly compare their mechanical responses under the same external load condition. From the perspective of equivalent loading ratios relative to their own rated working resistance, the loading ratio is 1.2 for the ZY6000 support and 1.125 for the ZY6400 support. This unified loading scheme allows for a fair comparison of the structural performance of the two supports under identical external excitation. Even under a higher relative loading ratio, the ZY6000 single-column support exhibits superior canopy mechanical performance, which further verifies the advantages of its canopy design. The limitation of this approach is that it does not directly compare the overload capacity of the two supports, which will be investigated in future research.

The transient impact load applied in all working conditions follows a two-stage time–force curve, as shown in Figure 7. The load increases linearly from 0 to the peak value of 7200 kN within 0.5 s, then remains constant for 0.5 s, with a total impact duration of 1.0 s. The loading rate is 1.44×10^4 kN/s, and the impact energy is calculated as 7.2×10^4 J based on the integral of force over displacement.

This loading parameter selection is based on the Chinese national standard GB 25974.1-2010 and relevant literature [13,15], which indicate that roof impact loads in underground coal mines include both fast transient impacts (20–50 ms) and slow progressive weighting impacts (0.5–2.0 s). The selected 1.0 s total duration corresponds to the typical slow roof weighting process in medium-thickness coal seams, which is the main service scenario of the ZY6000 and ZY6400 supports. This loading curve accurately reproduces the dynamic loading process caused by gradual roof subsidence and weighting.

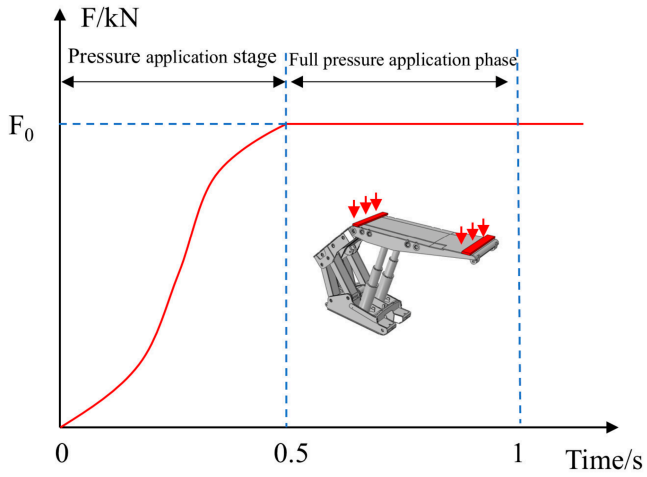

Figure 7. Time–load curve.

2.5. Setting of Safety Factor and Eccentric Angle

The structure is considered safe when $\sigma_{eq} \leq [\sigma]$, where $[\sigma]$ is the allowable stress of Q690 steel (690 MPa in this study). The safety factor "n" is defined as:

$$n = \frac{[\sigma]}{\sigma_{eq}} \tag{2}$$

A safety factor greater than 1 indicates that the structure is theoretically in the elastic deformation stage and no yield failure occurs based on the linear elastic material model. However, it should be noted that safety factors close to 1.0 indicate a limited safety margin, and the actual structural behavior may be affected by factors such as material defects and welding residual stress, which are not considered in this study.

Under eccentric operating conditions, the relative included angle between the offset position after compressing one side of the hydraulic support downward and the original position is defined as the initial angle θ (Figure 8). The initial angle θ can be derived using the tangent function, where "d" represents the width of the hydraulic support's canopy with a value of 1300 mm, and "h" denotes the maximum offset of the canopy.

$$tan\theta = \frac{h}{d} \tag{3}$$

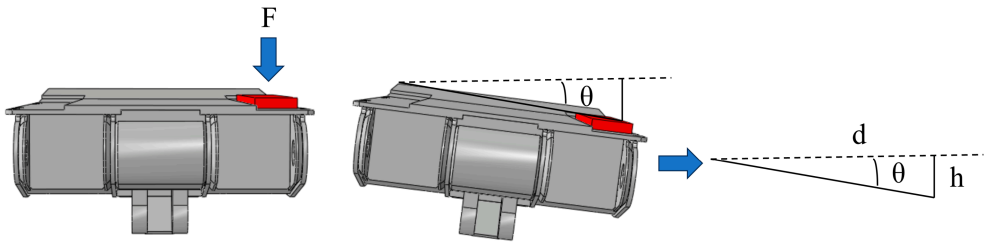

Figure 8. Schematic diagram of deflection angle for the canopy of hydraulic support.

3. Transient Dynamic Simulation Analysis of Hydraulic Unit Supports

3.1. Two-End Loading Condition of the Hydraulic Support Canopy

A concentrated force of 7200 kN is applied at the cushion blocks on both ends of the hydraulic support canopies to investigate the stress distributions of the two canopies. The stress distribution and displacement nephograms of the canopies under loading are presented in Figure 9. For the ZY6000 single-column shield hydraulic support, the maxi-

mum stress of the canopy reaches 535.9 MPa with a maximum displacement of 13.6 mm, both occurring at the central region of the canopy. By contrast, the ZY6400 double-column shield hydraulic support exhibits a maximum stress of 587.4 MPa and a maximum displacement of 13.9 mm, concentrating at the front-middle region of the canopy. After impact loading, obvious stress concentration appears at the structurally weak front section of the double-column support canopy. The canopy design of the single-column hydraulic support reduces the maximum stress by 8.77% and relocates the peak stress position to the structurally more stable central region.

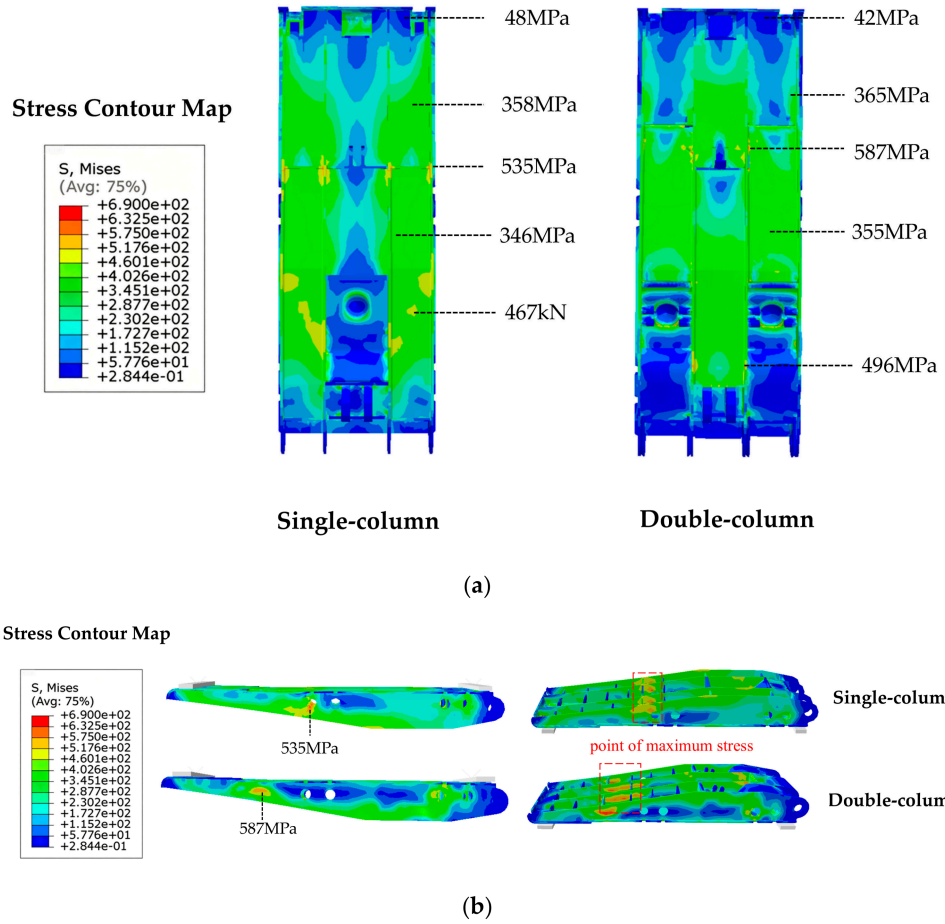

Figure 9. Stress nephograms of the canopies of two hydraulic supports under load conditions at both ends of the canopy. (**a**) Stress nephograms of the canopies of single-column hydraulic support and double-column hydraulic support. (**b**) Side view and bottom section view of the canopies of single-column hydraulic support and double-column hydraulic support.

The canopy of the hydraulic support constitutes the key component for which structural strength is of the highest priority in the entire support system. As depicted in Figure 10b, under impact loading, the stress and displacement in the central region of the canopy are considerably higher than those at both ends. As observed in Figure 10a, the time–stress curves of the two supports nearly coincide prior to 0.15 s. However, the stress fluctuation of the single-column hydraulic support begins to decay at approximately 0.25 s, and the stresses of both supports gradually converge to a stable state. As shown in Figure 9b, the mid-span displacement of the single-column support canopy is consistently lower than that of the double-column support throughout the loading process. Specifically, the maximum canopy displacement of the ZY6000 single-column support is 13.6 mm, which is 2.15% lower than that of the ZY6400 double-column support (13.9 mm). This

indicates that the single-column support exhibits better rigidity under canopy two-end loading conditions.

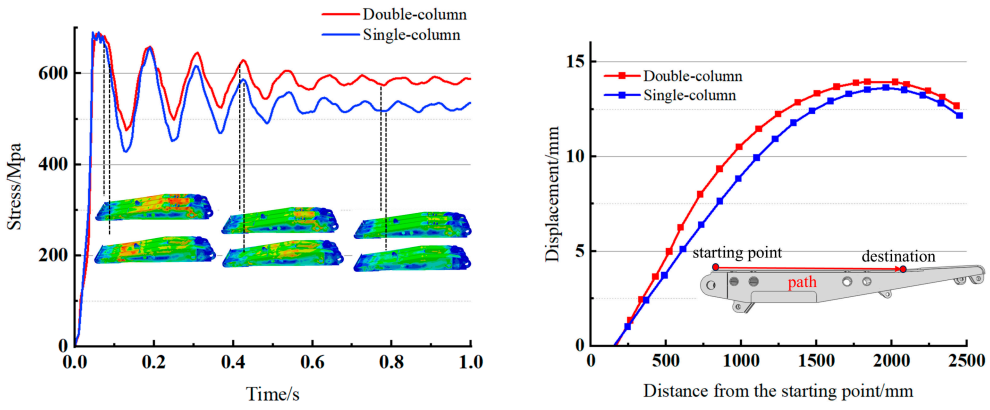

(**a**) (**b**)

Figure 10. Working condition of the hydraulic support canopy under compression at both ends. (**a**) Time–stress curve. (**b**) Displacement curve along the specified path of the canopy plate.

3.2. Two-End Loading Condition of the Hydraulic Support Base

The base of the hydraulic support acts as a critical load-bearing component within the entire support system. It sustains axial loads from the hydraulic props, transmits roof pressure and surrounding rock loads to the floor, and provides reliable support and anti-overturning stability for the entire support structure. Furthermore, the base ensures sufficient structural rigidity, resists floor deformation and uneven subsidence, and maintains the overall stability and service safety of the hydraulic support. Accordingly, in the strength evaluation of the single-column hydraulic support base, a comparative analysis is conducted with that of the double-column hydraulic support base.

As shown in Figure 11a, under impact loading, considerable stress occurs at the bent side plate of the column socket in the base of the single-column hydraulic support. The local maximum Mises stress reaches 646.9 MPa. The load transmission path is unique under the single-column loading mode, with high-stress zones concentrated, a large overall structural stress gradient, and significant stress concentration effects. The local maximum Mises stress of the double-column hydraulic support base is 475.8 MPa, approximately 26.4% lower than that of the single-column support. The double-column hydraulic support base is equipped with side protection plates, resulting in more uniform stress distribution, a significantly reduced range of high-stress zones, and an outstanding load homogenization effect.

Combined with the time–stress curve presented in Figure 12a, it is evident that the stress of the single-column hydraulic support base is significantly higher than that of the double-column hydraulic support base. Furthermore, the stress of the single-column hydraulic support base fails to stabilize within a short period, while the double-column hydraulic support base exhibits a small oscillation amplitude of the maximum stress after being subjected to the load and stabilizes at 475 MPa at approximately 0.25 s. As observed in Figure 12b, the positions of the maximum displacement for the two support bases are consistent; however, the maximum displacement of the single-column hydraulic support base is 0.68 mm larger than that of the double-column hydraulic support base. In conclusion, the design of the single-column hydraulic support base still requires further optimization. Specifically, side plate connections can be added to the base to achieve a more uniform stress distribution during loading.

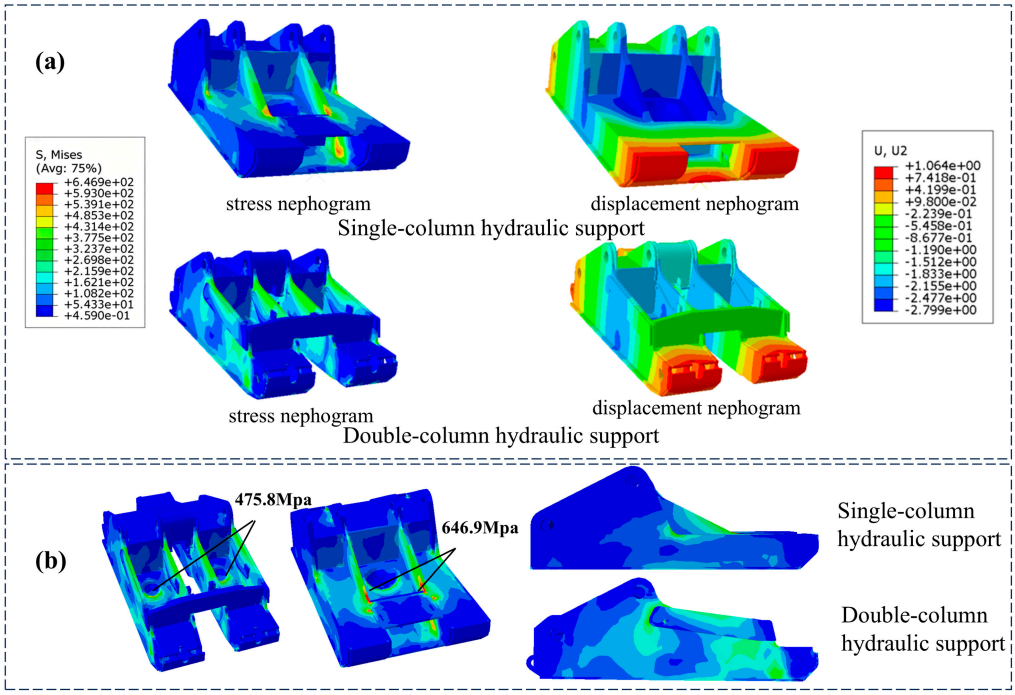

Figure 11. Stress nephograms and displacement nephograms of the base of two hydraulic supports under load conditions at both ends of the base. (**a**) Stress and displacement nephograms of the base of single-column hydraulic support and double-column hydraulic support. (**b**) Side view of the base of single-column hydraulic support and double-column hydraulic support.

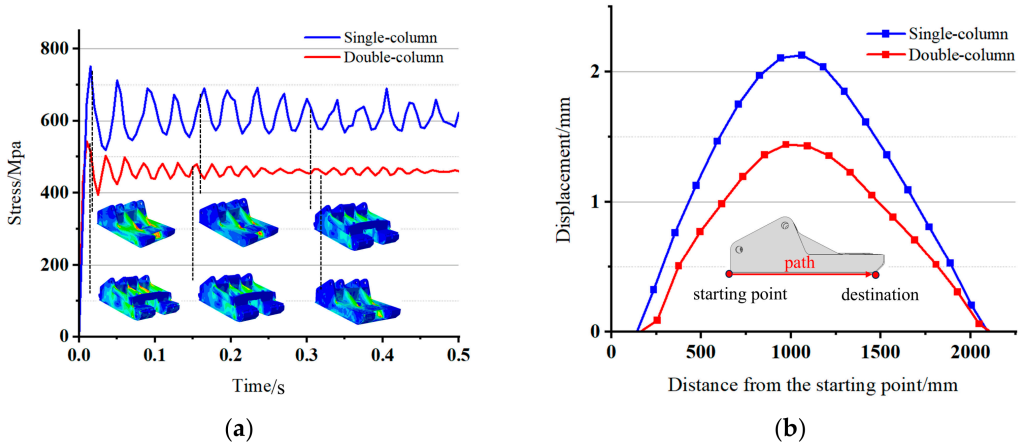

Figure 12. Working condition of the hydraulic support base under compression at both ends. (**a**) Time–stress curve. (**b**) Displacement curve along the specified path of the base.

3.3. Eccentric Compression of Hydraulic Support Canopy

Under certain extreme working conditions, when the hydraulic support performs supporting operations and its canopy comes into contact with an uneven roof, the canopy may bear unilaterally eccentric loads. Therefore, designs are carried out for the working condition of eccentric loads on the canopy to compare and analyze the stress states of the two types of supports. The simulation results of the hydraulic support under eccentric load conditions are shown in Figure 13: the entire hydraulic support displaces toward the side where the load is applied; the maximum displacement of the single-column hydraulic support is 25.8 mm, while that of the double-column hydraulic support is 27.1 mm; the deflection angle θ of the canopy of the single-column hydraulic support is calculated to be 1.134 degrees using Equation (3), and the deflection angle θ of the canopy of the double-

column hydraulic support is 1.191 degrees. Under identical load conditions, the canopy of the double-column support exhibits a larger deflection angle.

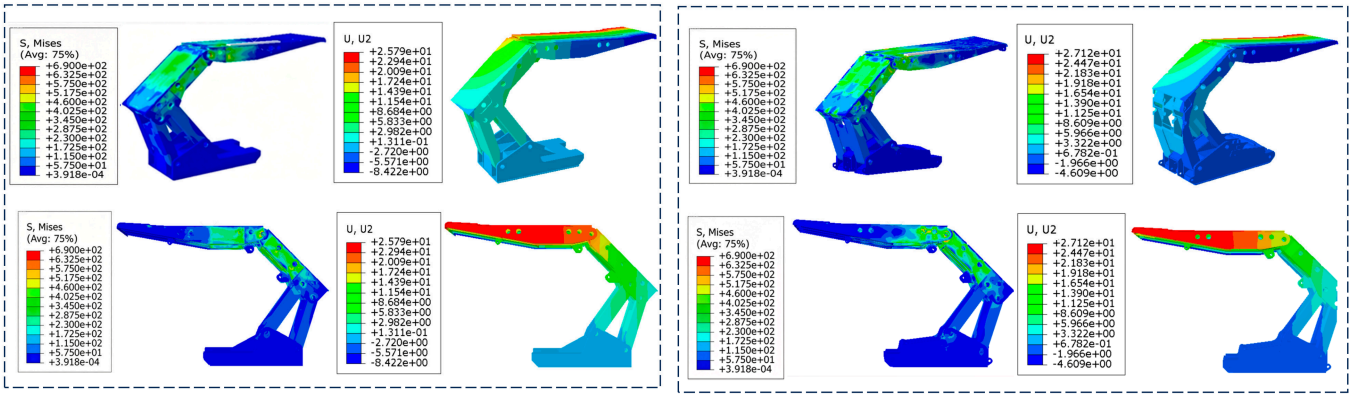

(**a**) (**b**)

Figure 13. Stress and displacement nephograms of hydraulic support under eccentric loading. (**a**) ZY6000 single-column shield hydraulic support. (**b**) ZY6400 double-column shield hydraulic support.

The stress of the canopy is mainly concentrated near the load application point, the connection between the canopy and the upright column, and the hinge joint between the canopy and the shield, showing an obvious stress concentration phenomenon. The stress of the shield is mainly concentrated at the hinge joint with the canopy. The eccentric load causes the shield to bear additional torque, resulting in an asymmetric stress distribution, with significant stress concentration at the hinge joint on the side close to the eccentric load.

It can be observed from Figure 14 that the maximum stress positions of the canopies of both are at the hinge joint between the canopy and the shield of the hydraulic support. The maximum stress of the canopy of the single-column hydraulic support is 658 MPa, and that of the double-column hydraulic support is 656 MPa. The two have the same maximum stress position and similar stress magnitude.

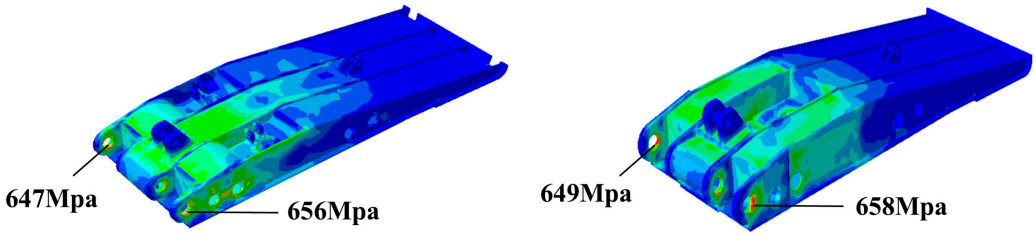

(**a**) (**b**)

Figure 14. The maximum stress position of the hydraulic support canopy under eccentric loading condition. (**a**) ZY6400 double-column shield hydraulic support. (**b**) ZY6000 single-column shield hydraulic support.

The shield beam is connected to the canopy via pins, causing the shield to twist to one side as the canopy rotates, with one side of the front end of the shield tilting upward. As can be seen in Figure 15, the maximum displacement of the shield of the single-column hydraulic support is 16.3 mm, and that of the double-column hydraulic support is 15.7 mm. The maximum stress of the shield of the single-column hydraulic support is 632.7 MPa, and that of the double-column hydraulic support is 635.2 MPa.

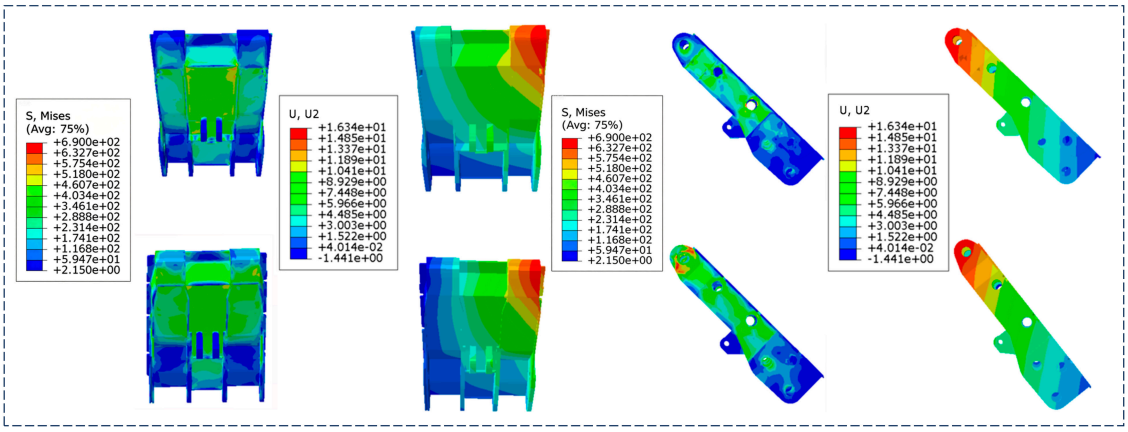

Figure 15. Displacement and stress nephograms of two hydraulic support shields at different angles.

It can be seen from Figure 16 that the maximum stress of the canopy for both hydraulic supports rapidly approaches 700 MPa under loading and then begins to decline at around 0.2 s. The single-column hydraulic support presents a more obvious stress reduction magnitude, with its minimum stress approximately 120 MPa lower than that of the double-column hydraulic support. Afterwards, the maximum stress of the canopy for both supports rebounds gradually without exceeding the peak value; meanwhile, the stress fluctuation of the single-column canopy is more prominent compared with the double-column structure.

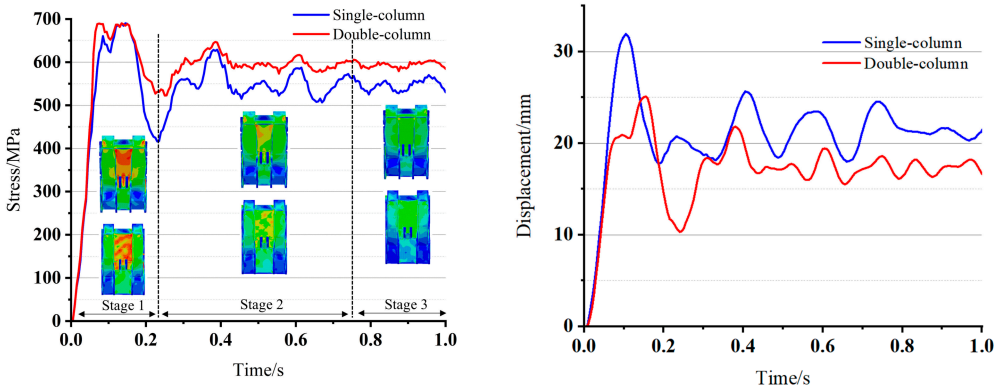

Figure 16. Eccentric compression condition of the shield of hydraulic support. (**a**) Time–stress curve. (**b**) Time-displacement graph.

Combining the displacement distribution of the canopy in Figure 12 with the deformation characteristics in Figure 16b, it is observed that when one side of the canopy of the single-column hydraulic support is subjected to downward compression, the opposite side of the canopy rotates upward via the hinge connection, resulting in an overall torsional deformation of the canopy. The upward displacement of the single-column canopy is notably larger than that of the double-column one. Before 0.2 s, an upward warping deformation occurs at one end of both canopies. Affected by the structural differences between the two support types, the maximum upward displacement of the single-column canopy is about 6 mm greater than that of the double-column counterpart.

In conclusion, the double-column hydraulic support possesses superior structural stability under eccentric loading. Although the single-column hydraulic support undergoes obvious stress and displacement fluctuations, it remains free of yield failure and can satisfy on-site support demands. All simulation data are summarized in Table 3.

Table 3. Simulation Data Sheet.

Working Condition	Maximum Stress/MPa	Maximum Displacement/mm	Maximum Stress Position	Safety Factor
End-loaded of canopy—Single Column	535.9	13.6	At the hole in the middle of the canopy	1.29
End-loaded canopy—Double column	587.4	13.9	Front end of the canopy	1.17
End-load of base—Single column	646.9	2.23	Bending side plate of the column socket	1.07
End-load of base—Double column	475.8	1.46	Column socket area	1.45
Eccentric Loading of Canopy—Single Column	658	25.8	Articulation between canopy and shield	1.05
Eccentric Loading of Canopy—Double Column	656	27.1	Articulation between canopy and shield	1.05
Eccentric Loading of Canopy—Shield of Single Column	632.7	16.3	At the web plate position of the shield	1.09
Eccentric Loading of Canopy—Shield of Double Column	635.2	15.7	At the web plate position of the shield	1.09

4. Model Optimization of ZY6000 Single-Column Shield Hydraulic Support

After analyzing the simulation data of the ZY6000 single-column shield hydraulic support based on the simulation data of the ZY6400 double-column shield hydraulic support, it is concluded overall that the single-column hydraulic support can meet the practical engineering requirements. Nevertheless, the base of the ZY6000 single-column support exhibits significant stress concentration, indicating room for further structural optimization. To address this issue, targeted optimization schemes were proposed with minimal cost increase, focusing on the canopy and base which are the main stress-concentrated components. The base optimization targets the bending side plate at the front weight-reducing region of the column socket, which is the dominant stress concentration area identified in the simulation. As shown in Figure 17, a smooth transition reinforcement structure is added at the front end of the weight-reducing base to improve the local force state. The detailed parameters are as follows:

4.1. Optimization Model Comparison of Canopy

The optimized hydraulic support canopy model is simulated under the working condition of Figure 6A, and the simulation data of the optimized canopy model and the initial canopy model are compared.

The design rationale of this optimization is to enhance the longitudinal structural continuity of the canopy by extending the top slab along the length direction of the support, so as to disperse the stress concentration at the middle hole and smooth the load transfer path. Notably, this optimization achieves a mass reduction of 92 kg (16.4% weight reduction for the top slab) while improving the stress distribution, which conforms to the lightweight design principle of mining support equipment.

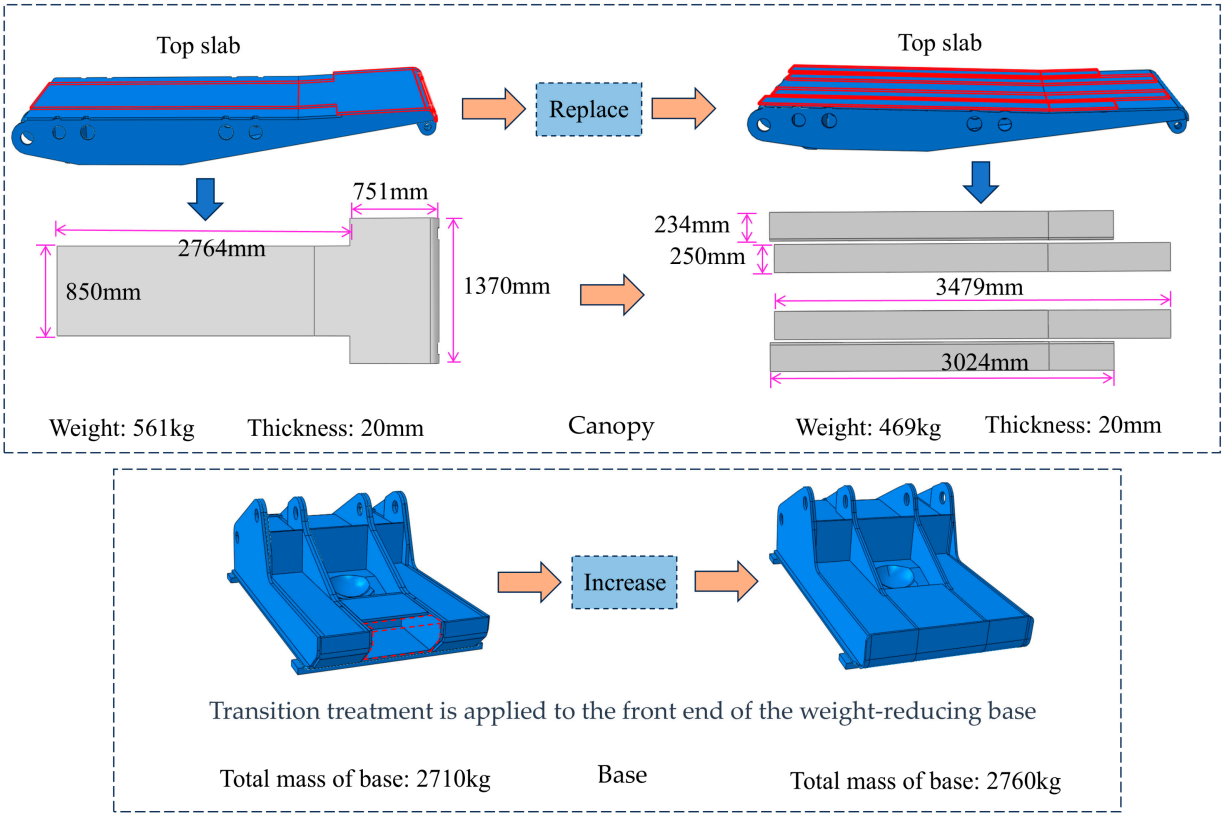

Figure 17. Schematic diagram for optimization of canopy and base of ZY6000 single-column hydraulic support.

As shown in Figure 18, the simulation results show that under the canopy two-end loading condition, the maximum stress of the optimized canopy is 526 MPa, which is 9.9 MPa lower than the original model (535.9 MPa), with a reduction rate of 1.85%. The maximum displacement of the canopy decreases from 13.6 mm to 13.3 mm, with a reduction rate of 2.21%. The safety factor increases from 1.29 to 1.31. The position of the maximum stress moves backward from the middle hole to the column socket area, which is a more stable structural position.

4.2. Optimization Model Comparison of Hydraulic Support Base

Simulations were conducted on the optimized hydraulic support base model under the working condition illustrated in Figure 6B, and the simulation results were compared with those of the original base model. As shown in Figure 19, under the base two-end loading condition, the maximum stress of the optimized base is 483 MPa, which is 163.9 MPa lower than the original model (646.9 MPa), with a significant reduction rate of 25.3%. The maximum displacement of the base decreases from 2.23 mm to 1.65 mm, with a reduction rate of 26.0%. The safety factor increases from 1.07 to 1.43, which greatly improves the structural safety margin.

In terms of mass and economic performance, the canopy top slab achieves a mass reduction of 92 kg (16.4% weight reduction) after structural optimization, while the base gains 50 kg (1.85% mass increase) due to the additional transition reinforcement structure. Overall, the total mass of the two optimized core components is reduced by 42 kg, realizing a lightweight design of the support.

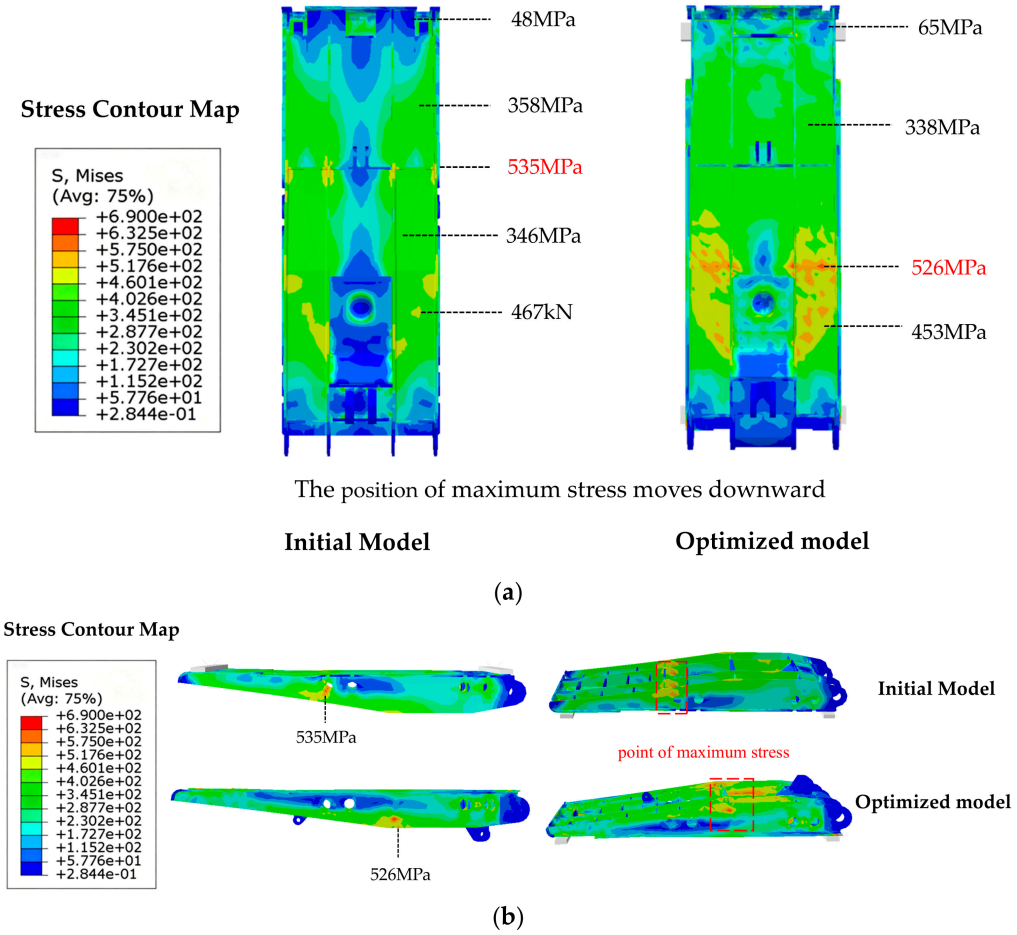

Figure 18. Stress cloud map of hydraulic support canopy under both-end loading condition. (**a**) Stress cloud map of the canopy of the initial model and the optimized model. (**b**) Side view and bottom section view of the canopy of the initial model and the optimized model.

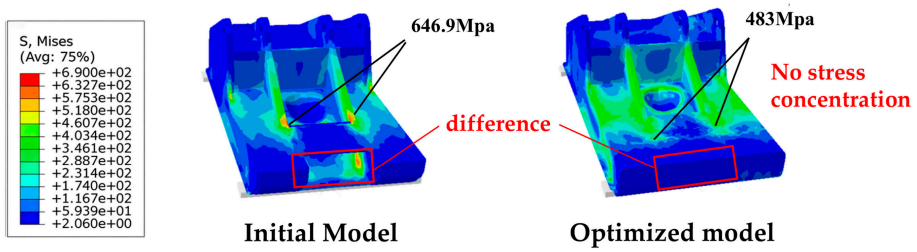

Figure 19. Stress cloud diagrams of the initial hydraulic support base model and the optimized hydraulic support base model.

According to the cost composition of hydraulic support products, steel material cost accounts for about 60% of the total manufacturing cost. The material cost saved by the lightweight canopy design can fully cover the increased material cost of the base reinforcement. Therefore, the total manufacturing cost of the optimized support is basically equivalent to that of the original model, with no additional cost increase, which meets the design goal of performance improvement under cost control.

To verify the universality of the optimization scheme, the optimized ZY6000 support model was also simulated under the canopy eccentric loading condition. The results, summarized in Table 4, show that under eccentric loading, the maximum stress of the optimized canopy is 642 MPa (2.43% reduction compared with 658 MPa of the original model), and the maximum stress of the optimized base is 552 MPa (5.96% reduction

compared with 587 MPa of the original model). These results confirm that the proposed optimization scheme is effective under all critical working conditions.

Table 4. Performance comparison before and after optimization of ZY6000 support.

Component	Working Condition	Original Maximum Stress/MPa	Optimized Maximum Stress/MPa	Original Safety Factor	Optimized Safety Factor
Canopy	Two-end Loading	535.9	526	1.29	1.31
Base	Two-end Loading	646.9	483	1.07	1.43
Canopy	Eccentric Loading	658	642	1.05	1.07
Base	Eccentric Loading	587	552	1.18	1.25

5. Conclusions

On the whole, the ZY6000 single-column shield hydraulic support has significant advantages in canopy bearing performance, manufacturing cost, lightweight level and hydraulic system simplicity. Its base load-bearing capacity and overall anti-eccentric stability are inferior to those of the double-column support, but after structural optimization, all performance indicators meet the requirements of relevant industry standards.

From the perspective of engineering application, for medium-thickness coal seams with inclination less than 15°, light load conditions and no strong rock burst risk, the single-column support has better comprehensive economic benefits and is more competitive in cost-sensitive mining scenarios. For working faces with large inclination, strong impact load or heavy bearing demand, the double-column support has more obvious advantages in stability and load-bearing redundancy.

1. Canopy Bearing Performance: Under the same load, the maximum stress and maximum displacement of the canopy of the ZY6000 single-column support are lower than those of the ZY6400 double-column support. The stress peak is located in the structurally more stable central area, indicating superior mechanical performance of the canopy.
2. Base Bearing Performance: Due to the single force transmission path, the single-column support base exhibits higher stress concentration, maximum stress and displacement than the double-column support. Structural optimization such as adding side plate connections is required to improve stress distribution.
3. Eccentric Load Adaptability: The maximum stress and its position of the canopies of the two supports are similar. The double-column support has stronger overall stability, while the single-column support does not exhibit theoretical yield failure under extreme eccentric conditions based on the linear elastic model and can meet basic support requirements. However, the safety margin is limited, and further optimization is recommended to improve structural reliability.
4. Replacing the original short integrated canopy top slab with four extended long slabs optimizes the canopy structure, reducing the maximum canopy stress by 1.85% and effectively shifting the peak stress position to the more stable column socket area at the rear of the canopy. Meanwhile, the top slab achieves a 16.4% weight reduction, realizing lightweight design. Adding a transition reinforcement structure at the front weight-reducing region of the base solves the stress concentration problem at the side plate bending position of the original model, with the maximum base stress reduced by 25.3%. The overall mass of the optimized support is slightly reduced, and the manufacturing cost is basically equivalent to the original model, achieving a good balance between mechanical performance improvement and lightweight design.

5. Comprehensive Application Value: The ZY6000 shield support unit meets the strength and deformation requirements for the three load variants under consideration to a degree comparable to that of the base support unit of the ZY6400 type. It has a cost advantage compared with double-column supports, is suitable for specific light-load coal mining faces, and possesses engineering promotion value.

This study mainly adopts the finite element transient dynamic simulation method to compare the mechanical performance of two types of hydraulic supports. Several limitations still exist in the current research. All analyses rely purely on numerical simulation, and no physical prototype tests or on-site field measurements are carried out to verify the accuracy of the simulation results. For future research, physical prototype experiments will be conducted to calibrate and validate the simulation model.

Author Contributions: D.A. and H.X. contributed to the conception of the study. Z.W., J.T. and R.T. carry out finite element modeling work. D.A. and Z.W. contributed significantly to analysis and manuscript preparation. D.A. and Z.W. performed the data analyses and wrote the manuscript. All authors have read and agreed to the published version of the manuscript.

Funding: This research was funded by the National Major Scientific Research Instrument Development Project (No.52427805).

Institutional Review Board Statement: Not applicable.

Informed Consent Statement: Not applicable.

Data Availability Statement: The original contributions presented in this study are included in the article. Further inquiries can be directed to the corresponding author.

Conflicts of Interest: The authors declare that they have no known competing financial interests or personal relationships that could have appeared to influence the work reported in this paper.

References

1. Hu, X.P.; Ji, X.D.; Liu, Y.; Du, Y. Study on Instability Mechanism of Hydraulic Support in Downdip and Updip Coal Face. *Alex. Eng. J.* **2023**, *81*, 304–318. [CrossRef]
2. Mu, M.F.; Xie, B.W.; Yang, Y. Research on Attitude Analysis of Hydraulic Support Based on Column Length. *Stroj. Vestn.* **2024**, *70*, 293–310. [CrossRef]
3. Xie, Y.Y.; Zeng, Q.L.; Jiang, K.; Meng, Z.S.; Li, Q.H.; Zhang, J.M. Investigation of Dynamic Behaviour of Four-Leg Hydraulic Support under Double-Impact Load. *Stroj. Vestn.* **2022**, *68*, 385–394. [CrossRef]
4. Yan, H.; Li, G.C.; Li, Y.Q.; Zhang, Q.C.; Zhu, C.Q. Stress Evolution Characteristics of the Intensively Mining-Induced Surrounding Roadways within an Extra-Thick Coal Seam: A Case Study from the Tashan Coal Mine, China. *J. Cent. S. Univ.* **2023**, *30*, 3840–3854. [CrossRef]
5. Qin, B.B.; He, F.L.; Zhang, Q.H.; Zhang, Z.J.; Sun, G.X.; Liu, X.H. Stability Evolution Mechanisms and Control Strategies for Lower and Upper Trapezoidal Blocks in Fully Mechanized Top-Coal Caving Faces of Extra-Thick Coal Seams. *Front. Earth Sci.* **2025**, *13*, 1586733. [CrossRef]
6. Guo, J.; Huang, W.B.; Feng, G.R.; Bai, J.W.; Li, L.R.; Wang, Z.; Yu, L.Y.; Wen, X.Z.; Zhang, J.; Feng, W.M. Stability Analysis of Longwall Top-Coal Caving Face in Extra-Thick Coal Seams Based on an Innovative Numerical Hydraulic Support Model. *Int. J. Min. Sci. Technol.* **2024**, *34*, 491–505. [CrossRef]
7. Hao, X.D.; Zhu, C.Z.; Zhang, J.J.; Ge, S.R.; Tian, K.; Gao, C. Position and Attitude Digital Twin Model of Hydraulic Supports in Fully Mechanized Workface. *Mech. Sci. Technol.* **2024**, *38*, 3741–3754. [CrossRef]
8. Liu, M.; Luan, B.H.; Xiao, Y. Energy Dissipation of Hydraulic Support Columns under Rockfall Impact Load in Steeply Dipping Coal Seams. *Processes* **2023**, *11*, 2497. [CrossRef]
9. Zeng, Q.L.; Xu, P.H.; Meng, Z.S.; Ma, C.; Lei, X.W. Posture and Dynamics Analysis of Hydraulic Support with Joint Clearance under Impact Load. *Machines* **2023**, *11*, 159. [CrossRef]
10. Cao, L.M.; Xu, Y.X.; He, C.; Zhang, E.M.; Miao, Y.F. Analysis of the Load-Bearing Characteristics of Hydraulic Supports for Top-Coal Caving under the Impact of Coal and Gangue. *Energy Sci. Eng.* **2024**, *12*, 4810–4822. [CrossRef]
11. Chen, H.; Yao, S.H.; Yang, Y.L.; Li, Y.F.; Xu, S.; Zhang, R.P. Fatigue Life Prediction of Aluminum Alloys Based on Surface and Internal Defects. *J. Mater. Eng. Perform.* **2023**, *32*, 8687–8699. [CrossRef]

12. Lei, X.W.; Meng, Z.S.; Zeng, Q.L.; Wan, L.R.; Ma, C. Study on the Operational Reliability of Hydraulic Support with Clearances Based on Mechanical-Hydraulic Interaction. *Ain Shams Eng. J.* **2026**, *17*, 104036. [CrossRef]
13. Wu, C.F.; Wu, T.G.; Zhao, L.J.; Li, W.L.; Zhang, Q.L.; Li, L.; Chen, Q. Research on Synchronous Load Control of Shield Beam for 50,000 Kn Hydraulic Support Test Bench. *PLoS ONE.* **2025**, *20*, e0335435. [CrossRef] [PubMed]
14. Dou, L.M.; Mu, Z.L.; Li, Z.L.; Cao, A.Y.; Gong, S.Y. Research Progress of Monitoring, Forecasting, and Prevention of Rockburst in Underground Coal Mining in China. *Int. J. Coal Sci. Technol.* **2014**, *1*, 278–288. [CrossRef]
15. Meng, Z.S.; Ma, C.; Xie, Y.Y. Influence of Impact Load Form on Dynamic Response of Chock-Shield Support. *Eksploat. Niezawodn.-Maint. Reliab.* **2023**, *25*, 168316. [CrossRef]
16. Meng, Z.S.; Zhang, J.M.; Xie, Y.Y.; Lu, Z.G.; Zeng, Q.L. Analysis of the Force Response of a Double-Canopy Hydraulic Support under Impact Loads. *Int. J. Simul. Model.* **2021**, *20*, 766–777. [CrossRef]
17. Wan, L.R.; Yu, X.H.; Ma, D.J.; Meng, Z.S.; Zeng, Q.L.; Qi, G.Q. Dynamic Response Analysis of a Novel Anti-Impact Pressure Balance Jack. *Energies* **2022**, *15*, 5236. [CrossRef]
18. Li, H.D.; Liu, Q.; Wang, C.L.; Shi, K.F.; Bao, X.P.; Song, X.Y.; Dong, Q.F. Magnetorheological Safety Valve and Control Strategies for Hydraulic Supports. *Appl. Sci.* **2026**, *16*, 1813. [CrossRef]
19. Liu, Y.; Liu, G.Z.; Li, J.X.; Zhen, Y.D.; Jiang, W. Study on the Dynamic Response Characteristics of Hydraulic Support Columns under Multi-Condition Impact Loads. *Front. Earth Sci.* **2026**, *13*, 1682976. [CrossRef]
20. Zhang, K.; Ma, K.L.; Zhang, Z.Y.; Cui, B.; Xu, Y.J.; Wei, X.T.; Chen, Y.; Zhang, Z.B.; Kong, X.J.; Chen, H.Y.; et al. Research and Experimental Verification of the Dynamic Pose Analysis Method of Advanced Hydraulic Support in a Fully Mechanized Mining Face. *Energy Sci. Eng.* **2025**, *13*, 3919–3934. [CrossRef]
21. Wang, K.Q.; Tian, X.H.; Chen, B.B.; Chen, X.R.; Wang, Q.Q.; Wang, J. Simulation Study on Dynamic Characteristics of Hydraulic Unit Support of Cyclic Self-Moving Combination Support. *Appl. Sci.* **2025**, *15*, 4480. [CrossRef]
22. Zeng, Q.L.; Ma, C.; Meng, Z.S.; Wang, J.T.; Xu, P.H.; Lei, X.W. Dynamic Response Difference of Hydraulic Support under Mechanical-Hydraulic Co-Simulation: Induced by Different Roof Rotation Position and Hysteresis Effect of Relief Valve. *Energies* **2023**, *16*, 159. [CrossRef]
23. *GB 25974.1-2010*; Powered Support for Coal Mine—Part 1: General Specification. General Administration of Quality Supervision, Inspection and Quarantine of the People's Republic of China: Beijing, China; Standardization Administration of China: Beijing, China, 2011.

Disclaimer/Publisher's Note: The statements, opinions and data contained in all publications are solely those of the individual author(s) and contributor(s) and not of MDPI and/or the editor(s). MDPI and/or the editor(s) disclaim responsibility for any injury to people or property resulting from any ideas, methods, instructions or products referred to in the content.